DOI: 10.1002/anie.201200845

Vaterite Structure

Ab Initio Structure Determination of Vaterite by Automated Electron Diffraction**

Enrico Mugnaioli, Iryna Andrusenko, Timo Schüler, Niklas Loges, Robert E. Dinnebier, Martin Panthöfer, Wolfgang Tremel, and Ute Kolb**

Many important and well-known materials, ranging from minerals or catalysts to framework compounds and pharmaceuticals, cannot be grown as single crystals. In these cases X-ray powder diffraction and pair distribution function analysis (PDF)[1] have been used for deriving the structural information that is fundamental for understanding material properties. Still, a number of compounds have eluded such kinds of analysis because they are nanocrystalline, highly disordered, with strong pseudosymmetries or available only in small amounts in polyphasic or polymorphic systems. These materials are crystallographically intractable with conventional X-ray or synchrotron radiation diffraction techniques.

Single nanoparticles can be visualized by high-resolution transmission electron microscopy (HR-TEM) up to sub-Ångstrom resolution,[2] but obtaining 3D information is still a difficult task, especially for highly beam-sensitive materials and crystal structures with long cell parameters. Electron diffraction (ED) delivers higher resolved data with a significant lower electron dose on the sample, but is biased by a substantial number of missing reflections and the occurrence of dynamic scattering that affects reflection intensities.[3] Therefore, ED is mainly used in combination with X-ray powder diffraction and high-resolution electron microscopy.[4]

Recently, an innovative approach for ED data acquisition and analysis, based on the combination of automated diffraction tomography (ADT)[5] and precession electron diffraction (PED)[6] could overcome traditional ED limitations and was shown to be an efficient routine for ab initio structure determination of structurally complex and beam-sensitive nanocrystalline phases.[7] The new strategy for ED data collection used in ADT can afford 3D diffraction data from a single nanocrystal (NC) down to a few tens of nanometers in size.[7d] Using non-oriented diffraction patterns with a tomographic scan of the reciprocal space, ADT provides almost complete and pseudo-kinematic reflection intensities from a single NC. Herein we demonstrate the power of the ADT approach by unveiling the structure of vaterite, the least stable anhydrous polymorph of $CaCO_3$, which has eluded structure determination for almost 100 years.

The scientific relevance of $CaCO_3$ is as wide-spread as its abundance. It plays a pivotal role in geosciences, biology, and industrial applications. Coral reefs and other geological chalk deposits bind an immense amount of carbon dioxide and thus regulate our climate.[8] $CaCO_3$ has been studied for more than a century[9] with more than 2000 publications during the past 10 years alone. It occurs in nature as anhydrous calcite, aragonite, and vaterite, and in hydrated forms as monohydrocalcite,[10] ikaite,[11] and amorphous $CaCO_3$.[12] Vaterite is a short-term weathering or biomineralization product. In spite of its abundance in natural and biological systems, its structure is still unknown. While calcite and aragonite form well defined single crystals, vaterite typically forms polycrystalline spherulites composed of nanosized crystallites (10–50 nm),[13] preventing any reliable structure determination to date. Recent reports about the stable prenucleation of ion clusters during the crystallization of calcium carbonate[14] sparked a discussion concerning the effect of nucleation on the subsequent polymorph selection. However, any understanding of the formation processes of the $CaCO_3$ polymorphs requires a knowledge of the crystal structures of all the polymorphs at the atomic level, as these determine physical properties, polymorph stability and crystal growth.[15]

All five previous structural models for vaterite derived from X-ray diffraction[16] show geometrically related cells that are difficult to distinguish on the basis of the low-quality data available for nanocrystalline vaterite. They propose a single carbonate CO_3^{2-} group in the asymmetric unit and mainly differ in its predicted site symmetry. Raman spectra provide controversial information, as vaterite is contaminated with other $CaCO_3$ polymorphs.[17] While Anderson[17a] supports Lippmann's model,[16d] Gabrielli et al.[18] are in favor of Meyer's second model.[16c] Wehrmeister et al.[17b] and Behrens et al.[19] claim that none of the proposed models is consistent

[*] Dr. E. Mugnaioli, I. Andrusenko, Dr. U. Kolb
Johannes Gutenberg-Universität Mainz
Institut für Physikalische Chemie
Jakob-Welder-Weg 11, 55128 Mainz (Germany)
E-mail: kolb@uni-mainz.de
T. Schüler, Dr. M. Panthöfer, Prof. Dr. W. Tremel
Johannes Gutenberg-Universität Mainz
Institut für Anorganische Chemie und Analytische Chemie
Duesbergweg 10–14, 55099 Mainz (Germany)
E-mail: tremel@uni-mainz.de
Dr. N. Loges
BASF Construction Chemicals GmbH
GMB/M-B08, 83308 Trostberg (Germany)
Dr. R. E. Dinnebier
Max-Planck-Institut für Festkörperforschung
Heisenbergstrasse 1, 70569 Stuttgart (Germany)

[**] This work was supported by the Deutsche Forschungsgemeinschaft (DFG) by grants SPP 1415 and SFB 625. N.L. was supported by POLYMAT, the graduate school of excellence of the state of Rhineland-Palatinate. We thank T. E. Gorelik, A. A. Stewart, and M. T. Otten for the ADT development and U. Heil, S. Schlitt, and E. Schömer for their cooperation in developing the ADT3D software.
Supporting information for this article is available on the WWW under http://dx.doi.org/10.1002/anie.201200845.

with the Raman spectra because they indicate the presence of two or more CO_3^{2-} groups in the asymmetric unit. NMR spectroscopy studies[20] of vaterite support a hexagonal symmetry but are not suitable for distinguishing the correct model. Recently, a new structure model for vaterite with hexagonal symmetry, a longer hexagonal axis and two CO_3^{2-} groups in the asymmetric unit was proposed based on molecular dynamic simulations and geometry optimization calculations.[21] Although none of the vaterite models is in accord with all experimental findings, some structural features are generally accepted: 1) the Ca atoms form a hexagonal sublattice; 2) all the CO_3^{2-} groups are oriented along the hexagonal axis; 3) the number of formula units per unit cell (Z) is at least 12; 4) the presence of only one CO_3^{2-} group in the asymmetric unit cannot explain the observed Raman spectra.

For the ADT/PED investigation two samples of synthetic vaterite, prepared by different routes, were analyzed. The first sample, prepared by mixing aqueous solutions of $Ca(NO_3)_2$ and Na_2CO_3,[22] mainly consisted of spherical aggregates of vaterite NCs with diameters of over 1 μm (Figure 1 a) and several micrometer sized crystals of calcite. After milling, isolated single crystals of vaterite with sizes of 50 nm or less

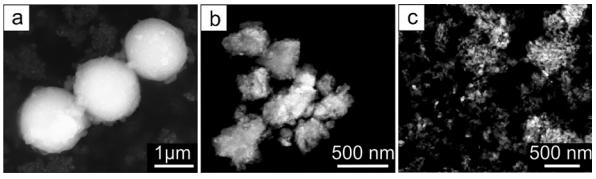

Figure 1. Scanning electron microscopy (SEM) and scanning transmission electron microscopy (STEM) overview images of vaterite NCs: a) SEM secondary-electrons image of typical spherical vaterite aggregates from the aqueous synthesis; b) dark-field STEM image of the same vaterite sample after ball-milling; c) dark-field STEM image of vaterite nanoparticles from the non-aqueous synthesis.

were found on the TEM grid and analyzed (Figure 1 b). The second vaterite sample, made by an independent non-aqueous approach,[23] consisted of aggregates with single domain sizes of up to 70 nm (Figure 1 c). Usually, vaterite crystals are aggregated in clusters of tens to thousands of individuals, but isolated NCs were found on the TEM grid (Supporting Information, Figure S1).

For both samples more than 10 independent ADT data sets were collected and reconstructed in 3D diffraction volumes (Figure 2) which were indexed to a monoclinic cell with parameters $a = 1.217$ nm, $b = 0.712$ nm, $c = 0.947$ nm, $\beta = 118.94°$. This cell is a geometric transformation of the smallest hexagonal cell proposed by Kamhi.[16b] The cell transformations from previous models to the cell derived by ADT data are illustrated in Figure S2 and Table S1. Despite the presence of residual dynamic scattering, systematic extinctions arising from C-centering were found down c^* axis and a c-glide plane orthogonal to b down a^*. Down b^* all general reflections (hkl) with $h \neq 3n$ were very weak and characterized by diffuse scattering along c^*.

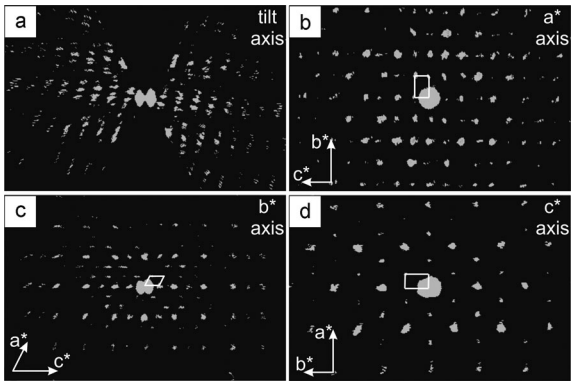

Figure 2. 3D reciprocal space reconstructed from ADT acquisition: a) view down the tilt axis; b) view down a^* axis; c) view down b^* axis; d) view down c^* axis. Note that these are projections of a 3D diffraction volume and not 2D oriented diffraction patterns.

The structure was determined independently from three ADT/PED data sets collected in tilt ranges of ±60° and 1° steps. The most important experimental parameters are listed in Table S2. The structure solution was performed ab initio by direct methods implemented in the program SIR2008[24] assuming the kinematic approximation, that is neglecting dynamic effects. In all three cases the structure solution converged to the same structure model in space group $C2/c$, $Z = 12$. The strongest 9 maxima in the potential map correspond to the 9 independent atoms of the structure and remaining maxima are negligible. Least-square refinement was performed with SHELXL97[25] imposing flat CO_3^{2-} groups and restraints of 0.128 nm on C–O distances and 0.222 nm on O–O distances. The final configuration, obtained after 30 cycles of refinement, was close to the structure obtained by direct methods (CIF file available in the Supporting Information). Atomic positions were stable and all atomic displacement parameters u were in the reliable range of 0.00036–0.00101 nm^2. The residual $R_1(4\sigma)$ was 37.61 %, a high value when compared with residuals of structure solutions from standard X-ray diffraction data, but within the expected range for ED refinements based on kinematic theory.[26] The correctness of the structure was assumed on the basis of the reproducibility and stability of the refinement. Figure 3 shows the final model along [010] and [103].

The structure contains most of the motifs present in previously reported models and exclusively explains all the features observed in the Raman spectrum and is isotypic with the high-temperature polymorph of $(Y_{0.92}Er_{0.08})BO_3$, previously described as a vaterite-like structure and recently solved in monoclinic symmetry by the use of neutron diffraction.[27] In contrast to calcite and aragonite, the two crystallographic distinct Ca^{2+} ions (8f and 4c site), and the two crystallographic distinct CO_3^{2-} ions (8f and 4e site) are separated in layers parallel to (001). The Ca^{2+} ions form distorted hexagonally packed planar arrangements that are interconnected by the CO_3^{2-} ions in a bridging mode. All planar trigonal CO_3^{2-} ions are aligned orthogonally to the planes containing the Ca^{2+} ions. Yet, the first set of CO_3^{2-} (1) ions is oriented with its twofold axis along the crystallographic b axis, while the

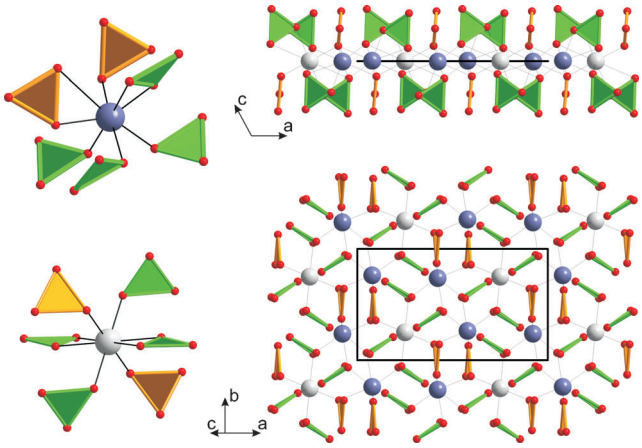

Figure 3. Vaterite crystal structure. Left: coordination of the Ca^{2+} ions (light gray: Ca(1); blue: Ca(2)) by the oxygen atoms of the two different carbonate groups (orange: CO_3^{2-}(1), green: CO_3^{2-}(2)). Right: views down [010] and [103] (equivalent to [001] in the previous hexagonal structure models) illustrating the layer type structure and the pseudohexagonal arrangement of the Ca^{2+} ions.

second set of CO_3^{2-} (2) ions is tilted with respect to *b*. This finding is in accordance with the reported optically positive character of vaterite, which was explained by the orthogonal orientation of the CO_3^{2-} ions to the basal (*a*,*c*) plane of the structure.[28] The presence of two crystallographic distinct CO_3^{2-} ions, with site symmetries C_2 (4*e*) and C_1 (8*f*) gives rise to three Raman active stretching modes, as reported for natural, biological, and synthetic vaterite samples from different origins.[17b]

In comparison with the previous models, the so-determined vaterite crystal structure exhibits a shift of the CO_3^{2-} ions layers along the *a* axis destroying the hexagonal symmetry. This structural peculiarity may give rise to a systematic merohedral twinning ("drilling") suggesting the hexagonal symmetry proposed before. It shows as well an unusual stacking of cation and anion layers along the [001] direction leading to an unfavorable Coulomb contribution to the lattice energy in comparison to calcite and aragonite. Thus, calcite and aragonite are stable polymorphs with well-defined stability regimes in the *p*,*T* phase diagram whereas vaterite is a metastable polymorph whose long-term stabilization is only possible as a biomineral hybrid or confined to boundary conditions, such as the nanosize regime.

The vaterite structure supports a number of experimental findings: 1) The density is lower than that of calcite/aragonite even though the Ca^{2+} coordination number (CN) is 8. 2) The higher surface charge of vaterite leads to stronger surface hydration, in particular in the presence of 3d transition metals, such as Cu^{2+} (CN = 6).[29] The preference of most 3d transition metals for sixfold coordination induces a transformation of vaterite into calcite, while a gradual replacement of Ca^{2+} with lanthanides (Ln^{3+}) stabilizes the vaterite polymorph. 3) The zeta potential is highly positive (Ca^{2+} surface layer), that of calcite is slightly negative.[30] The formation of vaterite under Langmuir monolayers is promoted by highly charged amphiphilic dendron–calixarene[31] or polymeric additives.[32] 4) Consequently, calcite prefers the adsorption of electrically neutral species whereas negatively charged species are adsorbed on vaterite. Under a sufficiently high CO_2 partial pressure the $CaCO_3$ crystallization is controlled kinetically, and vaterite is formed.[33]

Closer inspection of the 3D reconstructed diffraction volume shows diffuse scattering along *c**. Single oriented diffraction patterns collected along [010] reveal that general reflections (*hkl*) with $h \neq 3n$ exhibit a small non-rational shift along *c** of around $0.17 \cdot |c^*|$ (Figure 4a). The main periodicity is 0.83 nm (equivalent to d_{001}), but longer periodicities

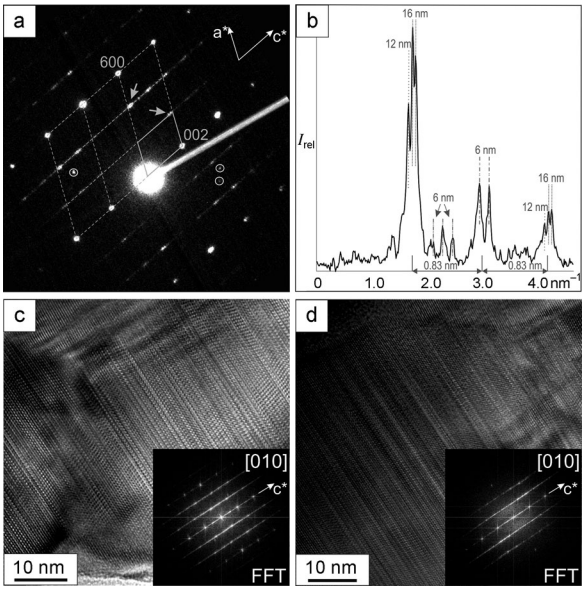

Figure 4. Diffuse scattering and local modulation along *c**: a) In-zone [010] nano electron diffraction (NED) patterns; the doubled reciprocal vectors are shown; reflections (*hkl*) with $h \neq 3n$ show diffuse scattering and a systematic small shift along *c** (marked with gray arrows); three foreign reflections are marked with circles; b) intensity profile taken along the 40*l* diffraction line, showing a main periodicity of 0.83 nm and other longer periodicities up to 16 nm; c) HRTEM image down [010] and related fast Fourier transform (FFT) showing disorder and local modulation along the *c** direction; d) HRTEM image down [010] and relative FFT showing a more disordered vaterite nanocrystal.

of 6, 12, and 16 nm (namely on the same order of magnitude of the crystal size) are also recognizable (Figure 4b). HRTEM images confirm the presence of a long-range stacking fault type disorder along the *c** direction, which locally can generate ordered modulated sequences (Figure 4c,d).

An exhaustive incommensurate structure analysis of vaterite is hampered by diffuse scattering, extra periodicities and a fast deterioration of the material under HRTEM conditions. At present, ADT data analysis is not able to provide conclusive quantitative information about disorder and incommensurate modulation even for larger domains and more stable phases.[7e,34] To understand the structural implication of the reflection shift along *c**, a larger cell with triple *c* periodicity was defined (Figure 5a). This setting is a close approximation of the postulated incommensurate modulation. The resulting cell parameters are: $a = 1.217$ nm, $b = 0.712$ nm, $c = 2.532$ nm, $\alpha = 90.00°$, $\beta = 99.22°$, $\gamma = 90.00°$.

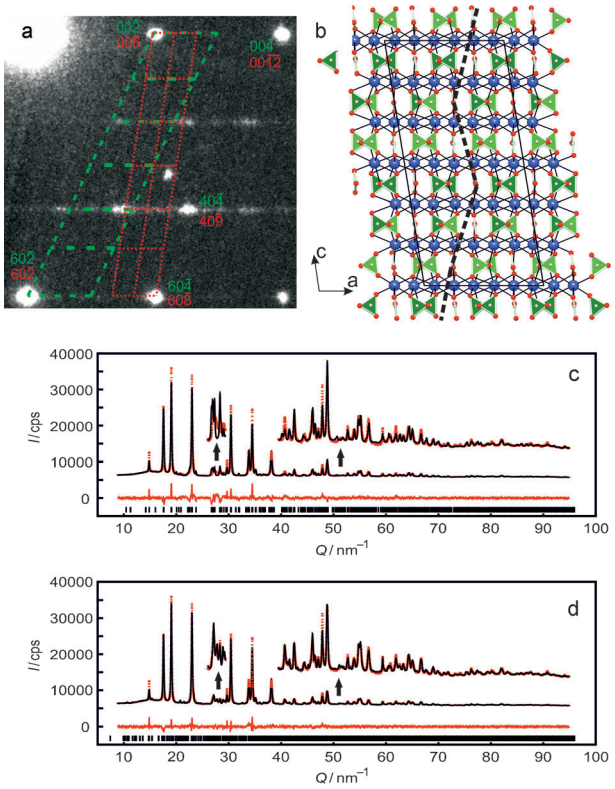

Figure 5. Vaterite six-layer triclinic model: a) section of a [010] diffraction pattern with a two-layer monoclinic cell (green) and six-layer triclinic cell (red) superimposed, exemplary reflections are indexed according to both the cells, 10*l* and 30*l* lines are extinguished because of the *C*-centering; b) [010] projection of the six-layer model (Ca blue, C gray, O red), the stacking vector is shown in black; c) Rietveld refinement (black line) of synchrotron data (red dots) and difference (red line) for the two-layer monoclinic model; d) Rietveld refinement for the six-layer triclinic model. cps = counts per second.

Intensities were extracted from the best ED volume (ADT data set III), collected on a nanoparticle obtained by the non-aqueous synthesis. The structure was solved ab initio by direct methods in the triclinic space group $C\bar{1}$. 45 of the 46 independent atoms of the structure were localized within the first 48 peaks of the charge-density maps, although most of them were light elements (C, O). The structure was refined imposing geometrical restraints on the CO_3^{2-} groups. The structure is similar to the two-layer monoclinic model described above with the same basic motif of Ca^{2+} layers connected by orthogonal CO_3^{2-} groups (Figure 5b and Figure S3). The local atom coordination is preserved; the main difference being the stacking sequence along *c* which changes from the simple sequence (+,+,...) to a sequence (+,+,−,+,+,−,...), where + and − indicate a shift of +1/3*a* and −1/3*a* every two anion layers.

High-resolution synchrotron powder diffraction data were collected on the more crystalline vaterite sample obtained from non-aqueous synthesis. Rietveld refinement based on the two-layer monoclinic model showed a moderately good fit but converge at relatively high residuals even for nanocrystalline samples (Figure 5c, Figure S2 and Table S3). In particular the scattering maxima at $Q \approx 27.5\ nm^{-1}$ and $Q \approx 37.4\ nm^{-1}$ were not modeled correctly. In contrast, the Rietveld refinement based on the triclinic six-layer superstructure converged at lower residuals and allowed a better fit of the diffractogram features (Figure 5d).

Reliable structure determinations based on X-ray diffraction for nanomaterials or compounds with complex structures available only as mixtures are very rare. Remarkably, the structure of vaterite was solved from ED data obtained by ADT from single crystals with a size not larger than 50 nm. The ADT structure model can explain the Raman spectra and all other experimental findings for vaterite. Aside from the average structure, an analysis of the 3D scattering volume revealed a structural modulation. Intensities extracted based on this modulation were used to determine the modulated superstructure ab initio.

Taking into account the inherent and not fully resolved drawback of dynamic scattering, electron-diffraction tomography showed its great potential for studying the structure of nanomaterials that elude conventional methods because of a small crystal size, low purity, structural complexity, or low availability. This powerful approach to structure solution can be straightforwardly applied to any type of polycrystalline material and is therefore pertinent to a diverse range of scientific disciplines.

Received: January 31, 2012
Revised: May 15, 2012
Published online: June 8, 2012

Keywords: biomineralization · calcium carbonate · electron crystallography · metastable phase · structure determination

[1] C. L. Farrow, S. J. L. Billinge, *Acta Crystallogr. Sect. A* **2009**, *65*, 232–239.
[2] a) K. H. Downing, M. Hu, H.-R. Wenk, M. A. O'Keefe, *Nature* **1990**, *348*, 525–528; b) C. Kisielowski, et al., *Microsc. Microanal.* **2008**, *14*, 469–477.
[3] D. L. Dorset, *Structural Electron Crystallography*, Plenum Press, New York, **1995**.
[4] a) S. Hovmöller, A. Sjögren, G. Farrants, M. Sundberg, B. O. Marinder, *Nature* **1984**, *311*, 238–241; b) C. Baerlocher, F. Gramm, L. Massüger, L. B. McCusker, Z. He, S. Hovmöller, X. Zou, *Science* **2007**, *315*, 1113–1116.
[5] a) U. Kolb, T. Gorelik, C. Kübel, M. T. Otten, D. Hubert, *Ultramicroscopy* **2007**, *107*, 507–513; b) U. Kolb, T. Gorelik, M. T. Otten, *Ultramicroscopy* **2008**, *108*, 763–772.
[6] a) R. Vincent, P. A. Midgley, *Ultramicroscopy* **1994**, *53*, 271–282; b) E. Mugnaioli, T. Gorelik, U. Kolb, *Ultramicroscopy* **2009**, *109*, 758–765.
[7] a) I. Rozhdestvenskaya, E. Mugnaioli, M. Czank, W. Depmeier, U. Kolb, A. Reinholdt, T. Weirich, *Mineral. Mag.* **2010**, *74*, 159–177; b) D. Denysenko, M. Grzywa, M. Tonigold, B. Streppel, I. Krkljus, M. Hirscher, E. Mugnaioli, U. Kolb, J. Hanss, D. Volkmer, *Chem. Eur. J.* **2011**, *17*, 1837–1848; c) J. Jiang, J. L. Jorda, J. Yu, L. A. Baumes, E. Mugnaioli, M. J. Diaz-Cabanas, U. Kolb, A. Corma, *Science* **2011**, *333*, 1131–1134; d) C. S. Birkel, E. Mugnaioli, T. Gorelik, U. Kolb, M. Panthöfer, W. Tremel, *J. Am. Chem. Soc.* **2010**, *132*, 9881–9889; e) I. Andrusenko, E. Mugnaioli, T. E. Gorelik, D. Koll, M. Panthöfer, W. Tremel, U. Kolb, *Acta Crystallogr. B* **2011**, *67*, 218–225; f) U. Kolb, T. E.

Gorelik, E. Mugnaioli, A. Stewart, *Polym. Rev.* **2010**, *50*, 385 – 409.
[8] R. E. Zeebe, J. C. Zachos, K. Caldeira, T. Tyrrell, *Science* **2008**, *321*, 51 – 52.
[9] J. W. Morse, R. S. Arvidson, A. Lüttge, *Chem. Rev.* **2007**, *107*, 342 – 381.
[10] H. Marschner, *Science* **1969**, *165*, 1119 – 1121.
[11] A. M. Shaikh, *J. Appl. Crystallogr.* **1990**, *23*, 263 – 265.
[12] M. Faatz, F. Gröhn, G. Wegner, *Adv. Mater.* **2004**, *16*, 996 – 1000.
[13] a) L. Brečević, V. Nöthig-Laslo, D. Kralj, S. Popović, *J. Chem. Soc. Faraday Trans.* **1996**, *92*, 1017 – 1022; b) J.-P. Andreassen, *J. Cryst. Growth* **2005**, *274*, 256 – 264.
[14] a) D. Gebauer, A. Völkel, H. Cölfen, *Science* **2008**, *322*, 1819 – 1822; b) E. M. Pouget, P. H. H. Bomans, J. A. C. M. Goos, P. M. Frederik, G. de With, N. A. J. M. Sommerdijk, *Science* **2009**, *323*, 1455 – 1458; c) D. Gebauer, P. N. Gunawidjaja, J. Y. P. Ko, Z. Bacsik, B. Aziz, L. Liu, Y. Hu, L. Bergström, C.-W. Tai, T.-K. Sham, M. Eden, N. Hedin, *Angew. Chem.* **2010**, *122*, 9073 – 9075; *Angew. Chem. Int. Ed.* **2010**, *49*, 8889 – 8891.
[15] N. H. de Leeuw, S. C. Parker, *J. Phys. Chem. B* **1998**, *102*, 2914 – 2922.
[16] a) H. J. Meyer, *Angew. Chem.* **1959**, *71*, 678 – 679; b) S. R. Kamhi, *Acta Crystallogr.* **1963**, *16*, 770 – 772; c) J. H. Meyer, *Z. Kristallogr.* **1969**, *128*, 183 – 212; d) F. Lippman, *Sedimentary Carbonate Materials*, Springer, New York, **1973**; e) A. Le Bail, S. Ouhenia, D. Chateigner, *Powder Diffr.* **2011**, *26*, 16 – 21.
[17] a) A. Anderson, *Spectrosc. Lett.* **1996**, *29*, 819 – 825; b) U. Wehrmeister, A. L. Soldati, D. E. Jacob, T. Häger, W. Hofmeister, *J. Raman Spectrosc.* **2010**, *41*, 193 – 201.
[18] C. Gabrielli, R. Jaouhari, S. Joiret, G. Maurin, *J. Raman Spectrosc.* **2000**, *31*, 497 – 501.
[19] G. Behrens, L. T. Kuhn, R. Ubic, A. H. Heuer, *Spectrosc. Lett.* **1995**, *28*, 983 – 995.
[20] D. L. Bryce, E. B. Bultz, D. Aebi, *J. Am. Chem. Soc.* **2008**, *130*, 9282 – 9292.
[21] J. Wang, U. Becker, *Am. Mineral.* **2009**, *94*, 380 – 386.
[22] A. Dandeu, B. Humbert, C. Carteret, H. Muhr, E. Plasari, J. M. Bossoutrot, *Chem. Eng. Technol.* **2006**, *29*, 221 – 225.
[23] T. Schüler, W. Tremel, *Chem. Commun.* **2011**, *47*, 5208 – 5210.
[24] M. C. Burla, R. Caliandro, M. Camalli, B. Carrozzini, G. L. Cascarano, L. De Caro, C. Giacovazzo, G. Polidori, D. Siliqi, R. Spagna, *J. Appl. Crystallogr.* **2007**, *40*, 609 – 613.
[25] G. M. Sheldrick, *Acta Crystallogr. Sect. A* **2008**, *64*, 112 – 122.
[26] a) T. E. Weirich, *Acta Crystallogr. Sect. A* **2001**, *57*, 183 – 191; b) H. Klein, *Acta Crystallogr. Sect. A* **2011**, *67*, 303 – 309.
[27] J. Lin, D. Sheptyakov, Y. Wang, P. Allenspach, *Chem. Mater.* **2004**, *16*, 2418 – 2424.
[28] C. W. Bunn, *Chemical Crystallography*, Clarendon Press, Oxford, **1946**.
[29] N. Nassrallah-Aboukaïs, A. Boughriet, J. Laureyns, A. Aboukaïs, J. C. Fischer, H. R. Langelin, M. Wartel, *Chem. Mater.* **1998**, *10*, 238 – 243.
[30] K. Sawada, *Pure Appl. Chem.* **1997**, *69*, 921 – 928.
[31] M. Fricke, D. Volkmer, C. E. Krill, M. Kellermann, A. Hirsch, *Cryst. Growth Des.* **2006**, *6*, 1120 – 1123.
[32] B. Aziz, D. Gebauer, N. Hedin, *CrystEngComm* **2011**, *13*, 4641 – 4645.
[33] S. R. Dickinson, G. E. Henderson, K. M. McGrath, *J. Cryst. Growth* **2002**, *244*, 369 – 378.
[34] L. Palatinus, M. Klementová, V. Dřínek, M. Jarošová, V. Petříček, *Inorg. Chem.* **2011**, *50*, 3743 – 3751.

